Available online at www.eccomasproceedia.org
Eccomas Proceedia COMPDYN (2017) 613-622

ECCOMAS
Proceedia

COMPDYN 2017
6th ECCOMAS Thematic Conference on
Computational Methods in Structural Dynamics and Earthquake Engineering
M. Papadrakakis, M. Fragiadakis (eds.)
Rhodes Island, Greece, 15–17 June 2017

NONSMOOTH SEISMIC RESPONSE ANALYSIS OF A BENCHMARK STRAIGHT BRIDGE WITH DECK-ABUTMENT IMPACT-INDUCED ROTATION

Zhongqi Shi[1] and Elias G. Dimitrakopoulos[2]

[1] The Hong Kong University of Science and Technology
Hong Kong Clear Water Bay, Kowloon, Hong Kong SAR, China
szqbell@gmail.com

[2] The Hong Kong University of Science and Technology
Hong Kong Clear Water Bay, Kowloon, Hong Kong SAR, China
ilias@ust.hk

Keywords: deck-abutment pounding, nonsmooth dynamics, friction, gap element, concrete bridges.

Abstract. *Deck-abutment contact, during earthquake excitation, might alter the boundary conditions at the deck level and activate a mechanical behavior unforeseen during the design of the bridge. Occasionally, this discrepancy between the assumed and the actual seismic behavior has detrimental consequences for the bridge e.g. pier damage, deck unseating or even collapse. A recent insightful shake-table test of a scaled deck-abutment bridge model [1], showed unexpected in-plane rotations even though the deck was straight. These contact-induced rotations produced significant residual displacements and damage to the piers and the bents. The present paper utilizes the measured response of the deck-abutment system to examine the validity of a proposed nonsmooth dynamic analysis framework. The results show that the proposed approach satisfactorily captures the planar rigid-body dynamics of the deck which is characterized by deck-abutment contact. Further, the study brings forward the role of friction on the physical mechanism behind the rotation of straight bridges. It underlines the importance of considering the frictional contact forces during deck-abutment interaction even for straight bridges, which are typically neglected. Finally, the paper comparatively assesses the nonsmooth approach vs. the compliance (or gap element) approach with respect to their ability to predict the measured response.*

Peer-review under responsibility of the organizing committee of COMPDYN 2017.
doi: 10.7712/120117.5444.18330

1 INTRODUCTION

A large number of bridges suffer damage due to contact (impact/pounding) during earthquake (e.g., [2]). Contact has direct consequences on bridges, such as local damage. More importantly though, contact can also alter the effective mechanical system of the bridge and even lead to deck unseating/collapse of the deck [3].

Of key importance to evaluate the seismic behavior of this type of bridge is the simulation of the deck-abutment pounding. Most studies adopt the gap element (compliance) approach, i.e., a spring with/without a dashpot activated only in compression after the clearance distance (gap) vanishes, solely along the normal direction of contact (e.g., [4], [5]). A limited number of studies consider the tangential contact forces due to friction when evaluating seismic behavior of the deck-abutment bridge system. An early exception is the study of Jankowski et al. [6] which adopts linear dashpot elements to simulate the tangential contact forces between the contacting bodies. More recently, Amjadian et al. [7] applied the Karnopp friction model to examine the response of curved bridges. Adopting an alternative nonsmooth dynamics approach, Dimitrakopoulos studied the pounding phenomenon between deck and abutment [8], [9], as well as between successive deck segments [10]. The analysis therein [9] also investigated the tendency of the deck to rotate after deck-abutment frictional/frictionless impact, and proposed the following dimensionless criteria:

$$\eta = \frac{\sin(2\alpha)}{2(W/L)} \pm 2\mu \frac{\cos^2 \alpha}{W/L} \tag{1}$$

where, μ is the coefficient of friction, α is the skew angle, W is the width, and L is the length of the deck, respectively (Figure 1). If $|\eta| > 1$, both a skew ($\alpha > 0$) and a straight ($\alpha = 0$) bridge will tend to rotate after deck-abutment impact, e.g., in Figure 1 (a) and (b) respectively. Saiidi et al. [1], performed large-scale shake table tests of a deck-abutment system and reported substantial, although unexpected, in-plane rotations of the deck, even though the bridge was straight. Among all potential rotation mechanisms, e.g. the stiffness eccentricity and the multi-support excitation, the frictional deck-abutment contact forces (and the torsional moment they produce) were identified [1] as the main reason of the deck rotation.

The present study uses the experimental data from [1] to validate a nonsmooth dynamics simulation and offer insight on the pounding-induced deck rotation. In this context, this study extends the nonsmooth dynamics framework proposed previously [8], [9], [10] to deal with the multi-support excitation, the inelastic behavior of concrete piers, and the continuous frictional contact of a multibody system. Finally, the present paper compares the nonsmooth approach with a conventional gap element (compliance) approach with respect to their ability to predict the observed deck response from [1].

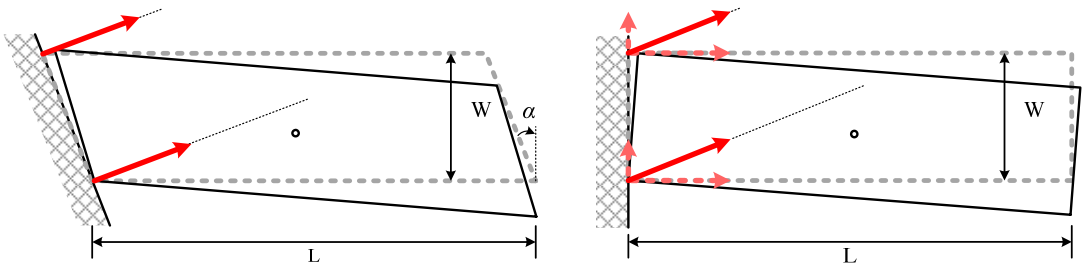

(a) frictionless contact of skew bridge ($\mu = 0$, $\alpha > 0$): $|\eta| > 1$ (b) frictional contact of straight bridge ($\mu > 0$, $\alpha = 0$): $|\eta| > 1$

Figure 1: Rotational mechanism due to deck-abutment pounding.

2 METHODOLOGY

This study compares the simulation results obtained by using different methods with the measured response of a 4-span reinforced concrete bridge (1/4-scale) model tested by Saiidi et al. [1]. The benchmark shake table tests concern a straight continuous post-tensioned deck supported by three 2-column bents and two abutment seats. Three independent shake tables introduce the ground accelerations along two translational directions at each bent base, while another two actuators controls the displacement of the abutment seats solely along the longitudinal direction. The seven sets of input excitations are scaled to different target Peak Ground Accelerations (PGAs). Of particular interest for the present study, are the deck-abutment pounding and the subsequent, but unexpected, in-plane rotation of the deck observed during these experimental tests.

2.1 Analytical model and equation of motion

The present study considers the idealized bridge model of Figure 2 which consists of 3 rigid bodies subjected to multiple-support excitation at the 3 bent supports ($\mathbf{u}_g^a$) and the 2 abutment seats ($\mathbf{u}_a^a$) [1]. The motion of the system is described by 7 degrees of freedom (DOFs) of the three rigid bodies (abutment seat '1' and '2' and the deck '*d*', discussed in [11]) with respect to an absolute reference frame (denoted with superscript '*a*'). The equation of motion for this multibody system with unilateral contacts and multiple-support excitation can be written as ([9], [11]):

$$\mathbf{M}\ddot{\mathbf{u}}^a - \mathbf{F}_D\left(\dot{\mathbf{u}}^r\right) - \mathbf{F}_S\left(\mathbf{u}^r\right) - \mathbf{W}_N\boldsymbol{\lambda}_N - \mathbf{W}_T\boldsymbol{\lambda}_T = 0 \tag{2}$$

where $\mathbf{M}$ is the mass matrix; $\ddot{\mathbf{u}}^a$ is the acceleration vector of the deck and the abutment seats with respect to an absolute system of reference (superscript '*a*'); $\mathbf{F}_D$ and $\mathbf{F}_S$ are the vectors of the damping and restoring forces, expressed using the relative veloci-

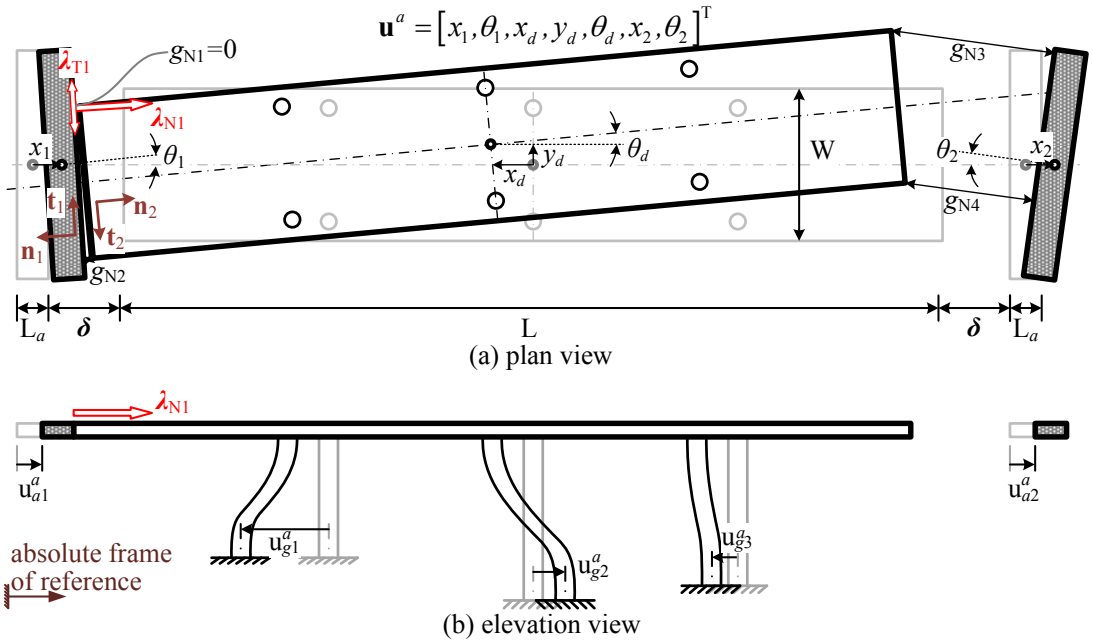

Figure 2: Kinematics and analytical model.

ty/displacement vector $\dot{\mathbf{u}}^r = \dot{\mathbf{u}}^a - \dot{\mathbf{u}}_g^a$ and $\mathbf{u}^r = \mathbf{u}^a - \mathbf{u}_g^a$ respectively; $\mathbf{W}_N$ and $\mathbf{W}_T$ are the direction matrices of the contact (constraint) forces in the normal (subscript '*N*') and the tangential (subscript '*T*') direction; $\boldsymbol{\lambda}_N$ and $\boldsymbol{\lambda}_T$ are the contact force vectors along the two directions of contact.

2.2 Nonsmooth dynamics

The proposed nonsmooth approach [8], [9], [10], [11] decomposes the dynamic response into continuous motion (without impacts) and discontinuous events [12], [13], [14]. In particular, it distinguishes contacts into *impacts* which are instantaneous events and *continuous contacts* of finite duration. Further, it enforces a kinematic ('impenetratability') constraint to ensure that the contacting deck and abutment cannot overlap. Lastly, it formulates [11] both types of contacts as pertinent Linear Complementarity Problems (LCPs, [15]). The following sections introduce briefly only the LCP for the impact. Refer to [8], [9], [10], [11] for the LCP treating continuous contact.

During impacts, the approach employs momentum-impulse principles to calculate the impulses transferred. Along the normal direction, Newton's law determines the normal contact velocity vector just after impact ($\dot{\mathbf{g}}_N^+$):

$$\dot{\mathbf{g}}_N^+ = -\bar{\bar{\boldsymbol{\varepsilon}}}_N \dot{\mathbf{g}}_N^- \tag{3}$$

where $\dot{\mathbf{g}}_N^-$ is the normal contact velocity vector just before impact, and $\bar{\bar{\boldsymbol{\varepsilon}}}_N = \mathrm{diag}\{\varepsilon_{Ni}\}$ with $\varepsilon_{Ni} \in [0, 1]$ being the coefficient of restitution of contact point *i*. As explained in [8], [9], [10], [11], the normal contact velocity vector $\dot{\mathbf{g}}_{N0} = \dot{\mathbf{g}}_N^+ + \bar{\bar{\boldsymbol{\varepsilon}}}_N \dot{\mathbf{g}}_N^-$ and the normal impulse $\boldsymbol{\Lambda}_N$ vector are complementary (see Eq. (7)).

Along the tangential direction of contact the positive $\dot{\mathbf{g}}_{TR}^+$ and the negative $\dot{\mathbf{g}}_{TL}^+$ parts of the tangential post-impact velocity $\dot{\mathbf{g}}_T^+$:

$$\dot{\mathbf{g}}_{TR} = \tfrac{1}{2}\left(|\dot{\mathbf{g}}_T| + \dot{\mathbf{g}}_T\right),\ \dot{\mathbf{g}}_{TL} = \tfrac{1}{2}\left(|\dot{\mathbf{g}}_T| + \dot{\mathbf{g}}_T\right),\ \dot{\mathbf{g}}_T = \dot{\mathbf{g}}_{TR} - \dot{\mathbf{g}}_{TL} \tag{4}$$

are complementary with the right $\boldsymbol{\Lambda}_{TR}$ and the left $\boldsymbol{\Lambda}_{TL}$ part of the Coulomb frictional impulse $\boldsymbol{\Lambda}_T$ (see also [8], [9], [10], [11]) respectively:

$$\begin{cases} \boldsymbol{\Lambda}_{TR} = \bar{\bar{\boldsymbol{\mu}}}\boldsymbol{\Lambda}_N + \boldsymbol{\Lambda}_T \\ \boldsymbol{\Lambda}_{TL} = \bar{\bar{\boldsymbol{\mu}}}\boldsymbol{\Lambda}_N - \boldsymbol{\Lambda}_T \end{cases} \tag{5}$$

where $\bar{\bar{\boldsymbol{\mu}}} = \mathrm{diag}\{\mu_i\}$ with μ_i being Coulomb's coefficient of friction of the *i*-th contact.

The LCP which treats frictional single and multiple impacts is:

$$\begin{pmatrix} \dot{\mathbf{g}}_{N0} \\ \dot{\mathbf{g}}_{TR}^+ \\ \boldsymbol{\Lambda}_{TL} \end{pmatrix} = \begin{pmatrix} \mathbf{G}_{NN} - \mathbf{G}_{NT}\bar{\bar{\boldsymbol{\mu}}} & \mathbf{G}_{NT} & \mathbf{0} \\ \mathbf{G}_{TN} - \mathbf{G}_{TT}\bar{\bar{\boldsymbol{\mu}}} & \mathbf{G}_{TT} & \mathbf{E} \\ 2\bar{\bar{\boldsymbol{\mu}}} & -\mathbf{E} & \mathbf{0} \end{pmatrix} \begin{pmatrix} \boldsymbol{\Lambda}_N \\ \boldsymbol{\Lambda}_{TR} \\ \dot{\mathbf{g}}_{TL}^+ \end{pmatrix} + \begin{pmatrix} \left(\bar{\bar{\boldsymbol{\varepsilon}}}_N + \mathbf{E}\right)\dot{\mathbf{g}}_N^- \\ \dot{\mathbf{g}}_T^- \\ \mathbf{0} \end{pmatrix} \tag{6}$$

with complementary conditions:

$$\begin{pmatrix} \dot{\mathbf{g}}_{N0} \\ \dot{\mathbf{g}}_{TR}^{+} \\ \boldsymbol{\Lambda}_{TL} \end{pmatrix} \geq \mathbf{0}, \begin{pmatrix} \boldsymbol{\Lambda}_{N} \\ \boldsymbol{\Lambda}_{TR} \\ \dot{\mathbf{g}}_{TL}^{+} \end{pmatrix} \geq \mathbf{0} \text{ and } \begin{pmatrix} \dot{\mathbf{g}}_{N0} \\ \dot{\mathbf{g}}_{TR}^{+} \\ \boldsymbol{\Lambda}_{TL} \end{pmatrix}^{\mathrm{T}} \begin{pmatrix} \boldsymbol{\Lambda}_{N} \\ \boldsymbol{\Lambda}_{TR} \\ \dot{\mathbf{g}}_{TL}^{+} \end{pmatrix} = \mathbf{0} \tag{7}$$

where, the **G** matrices are

$$\begin{aligned} \mathbf{G}_{NN} &= \mathbf{W}_{N}^{\mathrm{T}} \mathbf{M}^{-1} \mathbf{W}_{N}, \quad \mathbf{G}_{NT} = \mathbf{W}_{N}^{\mathrm{T}} \mathbf{M}^{-1} \mathbf{W}_{T} \\ \mathbf{G}_{TN} &= \mathbf{W}_{T}^{\mathrm{T}} \mathbf{M}^{-1} \mathbf{W}_{N}, \quad \mathbf{G}_{TT} = \mathbf{W}_{T}^{\mathrm{T}} \mathbf{M}^{-1} \mathbf{W}_{T} \end{aligned} \tag{8}$$

3 ANALYTICAL RESULT

To replicate the experimental testing procedure of Saiidi et al. [1], the analytical model of the deck-abutment seats system of Figure 1 is subjected successively to the same seven excitations. The two abutment seats are constrained to the measured motion which is now used as input to the system. The concentrated mass at the center of the deck and the mass moment of inertia is m_d = 140.5 t and I_d = 13090 t·m^2. The nonlinear behavior of the RC columns is modeled with Takeda hysteretic models [16] in both the longitudinal and the transverse directions. The coefficient of restitution is assumed $\varepsilon_N = 0.0$ and the coefficient of friction is μ = 0.5. The damping is modelled with a Rayleigh damping matrix, assuming 8% damping coefficient for the first and the third mode.

3.1 Nonsmooth seismic response analysis

This subsection presents the calculated response based on the proposed nonsmooth approach. The comparison between the experimental and the analytical results is based on the

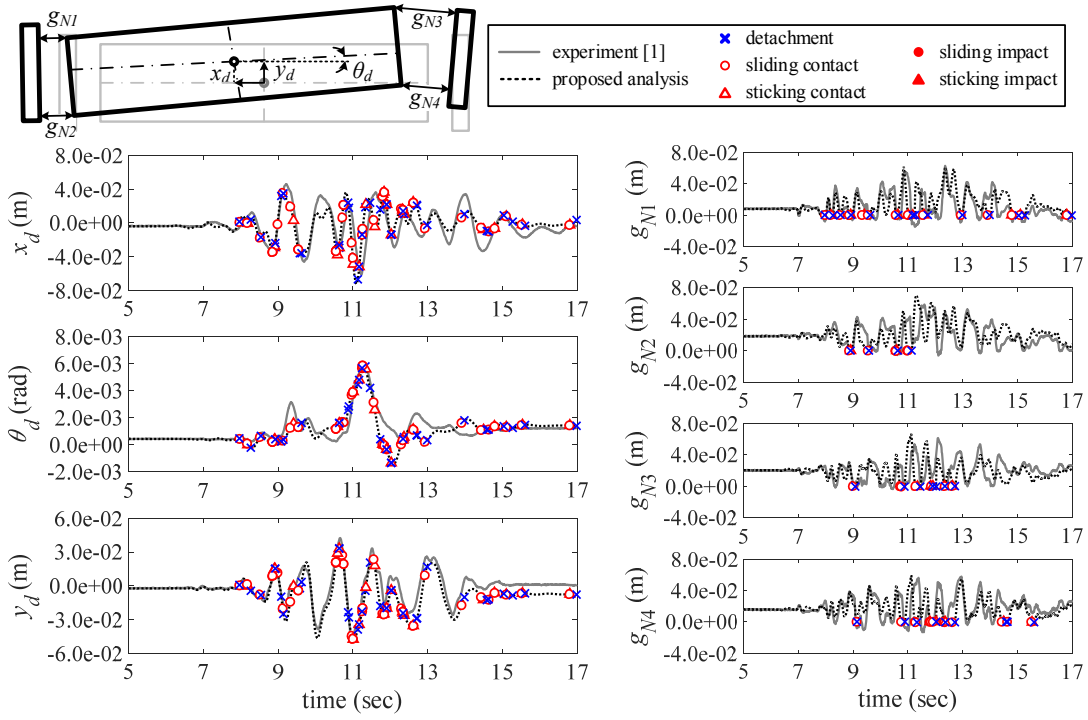

Figure 3: Comparison of response-history under Excitation No. 5: experiment [1] versus proposed analysis.

following calculation assumptions: the longitudinal displacement of the deck is the average of the measurements at the two ends of the deck, the transverse displacement is the one measured at the middle of the deck, and the deck in-plane rotation is obtained from the two transverse displacements measured at the two ends (along the length) of the deck. Figures 3 ~ 5 compare the response measured experimentally with that calculated analytically under Excitation No. 5 as an example. A summary of all 7 excitations follows later on (Figure 6).

Figure 3 illustrates the response histories of the two translational displacements x_d and y_d and the rotation θ_d of the deck (left) and the relative distance between the four corners of the deck and the adjacent abutment seats $g_{N1} \sim g_{N4}$ (right). The figure also depicts the different types of contact events at all 4 contact points. The proposed nonsmooth approach reproduces very well the observed response of the deck for both the longitudinal and the transverse directions despite the numerous contact events between the deck and the abutment seats. Under Excitation No. 5, it also satisfactorily reproduces not only the experimentally observed peak rotation, but also the trend of the recorded rotations. This is a particularly challenging task since the deck response is dominated by frictional contact.

Figure 4 compares the response history of the angular velocity during Excitation No. 5. Again, the proposed analysis replicates the general trend of the angular velocity variation, although some discrepancies are noted in terms of peak values as well as response history. To bring forward the underlying physics of the rotation mechanism, Figure 4 also illustrates a continuous sliding contact (8.98 ~ 9.08 sec), at point 3. Figure 5 plots the deformation of the deck-abutment system and the analytically calculated contact forces at the beginning of this continuous contact. At t = 8.98 sec, the normal contact force λ_{N3} = 144 kN produces clockwise moment, and the tangential contact forces λ_{T3} = 72 kN produce anticlockwise moments.

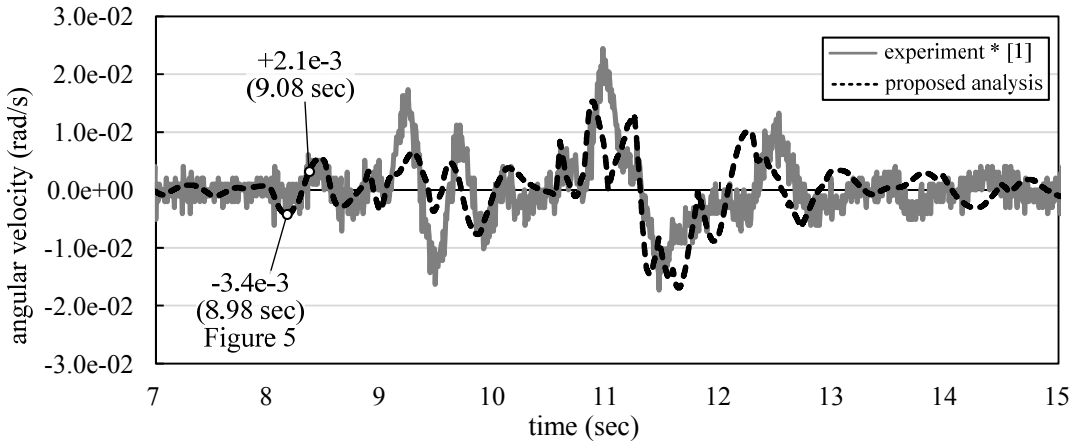

Figure 4: Comparison of angular velocity history under Excitation No. 5: experimental result [1] (*: calculated from the numerical time differentiation of the recorded deck displacements) versus proposed analysis.

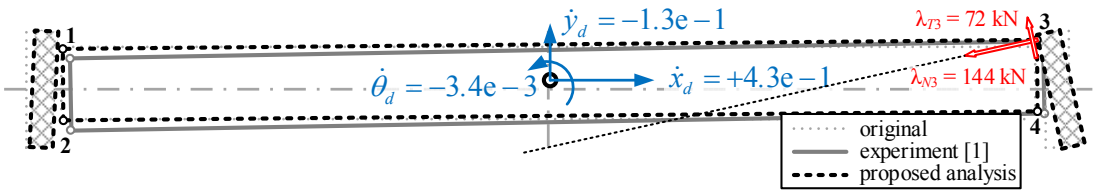

Figure 5: Comparison of deck response at 8.98 sec under Excitation No. 5: experimental result [1] (deformation only) versus proposed analysis (deformation, response velocities, contact forces).

Due to the rotated right abutment seat, the normal and tangential direction of this contact also rotate. As a result, the angular velocity increases from $\dot{\theta}_d(8.98) = -3.4 \cdot 10^{-3}$ rad/s to $\dot{\theta}_d(9.08) = +2.1 \cdot 10^{-3}$ rad/s. This indicates the dominant role of the frictional contact force on the in-plane rotation of the deck.

In summary, Figure 6 plots the peak deck rotation versus the target transverse PGA for all 7 excitations. Based on the experimental tests, the peak deck rotation increases exponentially with respect to the input PGA [1]. The proposed nonsmooth approach well reproduces this tendency with reasonable accuracy. The analysis underestimates the peak deck rotations under Excitations No. 6 and 7. Note though that, both the possible local damage due to extensive excitations (the target transverse PGA is as high as 1.0 g), as well as, the uncertain coefficient of friction (the value assumed herein is a constant 0.5) may introduce some error into the simulation, as discussed in [11]. On the other hand, the peak deck rotation ignoring the deck-abutment pounding is notably smaller than both the experimental results and the analytical results taking into account the deck-abutment pounding.

4 COMPARISON WITH GAP ELEMENT APPROACH

4.1 General and analytical condition

Most numerical/analytical studies of the pounding phenomenon adopt the gap element ('compliance') approach (e.g. [4] ~ [7]). This section compares the compliance and the non-smooth approaches with respect to their ability to simulate the deck response recorded during the shake table tests [1], especially the in-plane rotation. Here, the compliance approach adopts the same analytical model as Subsection 2.1, but uses the spring-dashpot gap element at four corners of the deck to simulate the deck-abutment pounding. The contact force vectors ($\boldsymbol{\lambda}_N$ and $\boldsymbol{\lambda}_T$) enter the equation of motion (Eq. (2)) where the gap of point i closes (the relative distance becomes smaller than zero: $g_{Ni} < 0$). Based on the Hertz-damp model and Coulomb's law, the contact force along the normal and the tangential direction is respectively:

$$\lambda_{Ni} = \begin{cases} 0, & g_{Ni} \geq 0 \\ -k\left(g_{Ni}\right)^{1.5} - c\dot{g}_{Ni}, & g_{Ni} < 0 \end{cases} \tag{9}$$

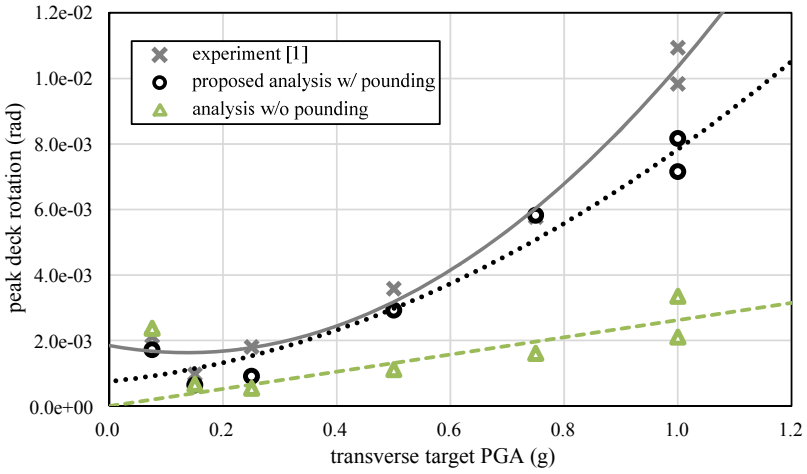

Figure 6: Summary of peak deck rotation versus target transverse PGA under all 7 excitations.

$$\lambda_{Ti} = \begin{cases} -\mu \operatorname{sgn}\left(\dot{g}_{Ti}\right)\lambda_{Ni}, & \left|\dot{g}_{Ti}\right| \geq \varepsilon \\ -\left(\left|\dot{g}_{Ti}\right|/\varepsilon\right)\mu \operatorname{sgn}\left(\dot{g}_{Ti}\right)\lambda_{Ni}, & \left|\dot{g}_{Ti}\right| < \varepsilon \end{cases} \tag{10}$$

where, k and c is the stiffness and the damping of the gap element, respectively, ε (= 10^{-3} m/s) is a scalar parameter which determines the sticking-sliding transition. This study adopts the proposed stiffness and damping values of [17], [18], [19], and also examines other values of stiffness ranging from 10^{-4} to 10^{+2} k.

4.2 Comparison of analytical results

Figure 7 plots the response history of the translational displacements and the in-plane rotation of the deck during Excitation No. 5. For the longitudinal displacement of the deck, all analytical results replicate the general trend observed in the experimental tests. When the stiffness is small (10^{-4} ~ 10^{-2} k), the results present some minor differences in terms of response history, but the peak displacements are in agreement. For the transverse displacements, both the nonsmooth and the compliance approaches are in good agreement with the experiment. However, the two approaches generate notable discrepancies in terms of the in-plane rotation history of the deck. The rotation calculated by the nonsmooth approach matches better the experimental results, in not only the overall response history but also the peak deck rotation. In general, when adopting relatively large stiffness values (10^{0} ~ 10^{+2} k), the compliance approach can produce similar trends of the in-plane rotation. On the contrary, when using small stiffness values (10^{-4} ~ 10^{-2} k), the compliance approach fails to simulate the rotational motion of the deck. The comparison under the other 6 excitations shows similar ob-

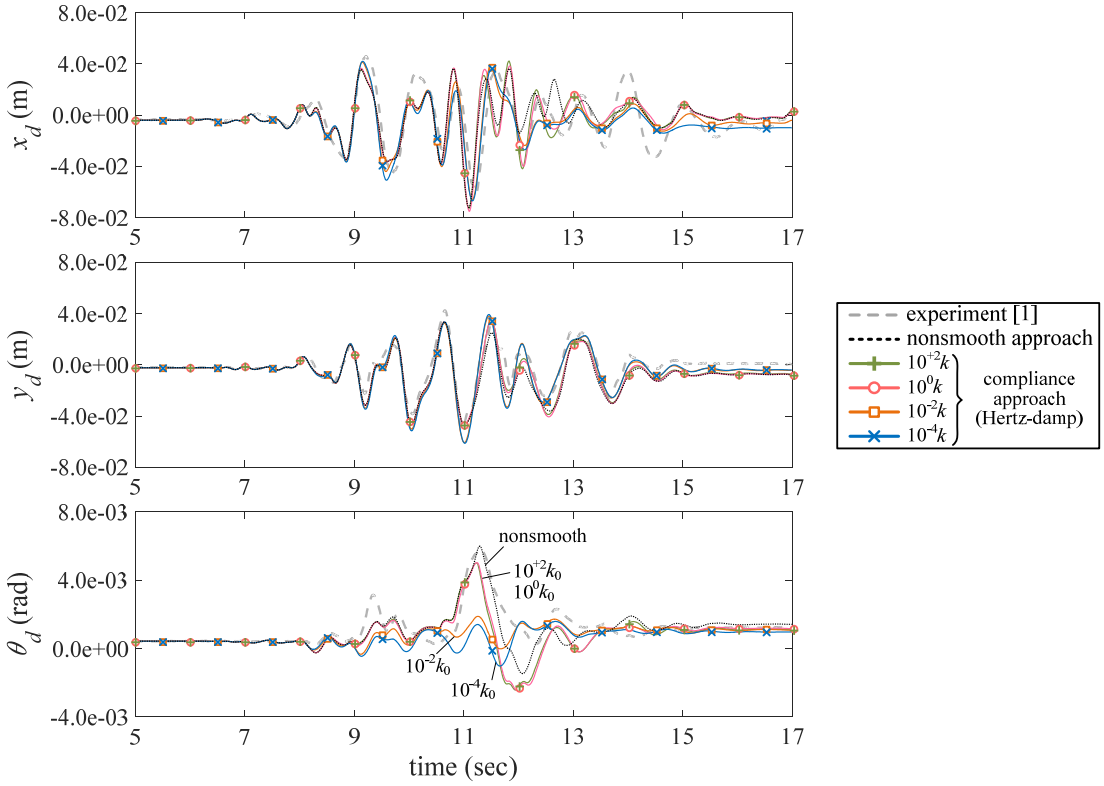

Figure 7: Comparison of response-history under Excitation No. 5: proposed analysis versus compliance approach

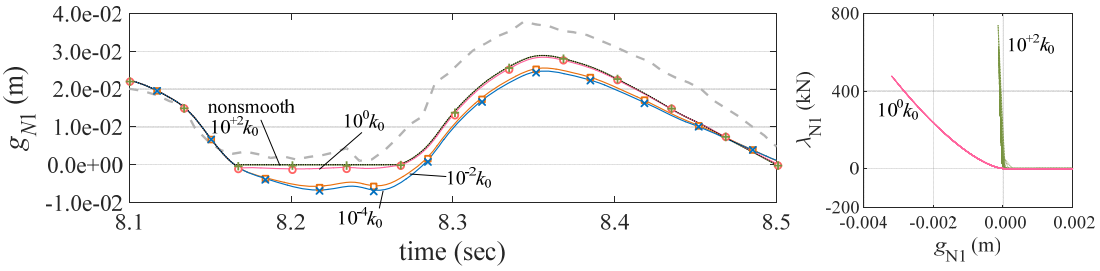

Figure 8: Influence of contact stiffness: (left) response history of the relative distance; (right) force-displacement loop of the gap element.

servation, and is omitted here for brevity.

To better understand these discrepancies, Figure 8 illustrates (left) the response history of the relative distance at point 1 (g_N1) during the first pounding (at about 8.17 sec) under Excitation No. 5 and (right) the force-displacement loops of the pertinent gap element ($10^0\ k$ and $10^{+2}\ k$ as an example). The compliance simulation with large stiffness value ($10^{+2}\ k$) approximates the impenetrability constraint and, subsequently, generates similar results to the nonsmooth analysis. From Figure 8 left, the lower the contact stiffness, the larger the penetration and the longer the contact duration. Such influence accumulates and significantly affects the in-plane rotation history. Figure 8 right shows the obvious discrepancy between the force-displacement loops when using two different stiffness values. The smaller stiffness leads to larger penetration and smaller normal contact force, and consequently the smaller tangential contact force (friction, Eq. (10)) and torsional moment.

5 CONCLUSIONS

The present paper proposes a nonsmooth dynamics simulation of the seismic response of bridge involving deck-abutment pounding. The comparison with benchmark experiment results shows good match, not only in terms of the two translational displacements but also, and most importantly, in terms of the in-plane rotation of the deck. The analytical results replicate the experimentally observed trend where the peak deck rotation increases exponentially with respect to the input PGA. The study also sheds light on the crucial role of friction on the deck-abutment pounding problem. Considering only frictionless contact may significantly underestimate the planar response of the deck.

Furthermore, this study compares the proposed nonsmooth approach and the widely used compliance (gap element) approach, particularly with respect to their ability to replicate the experimental response. The in-plane deck rotation is notably sensitive to the contact stiffness of the gap element. Adopting relatively large contact stiffness for the Hertz-damp model generates satisfactorily similar results compared with the nonsmooth approach. On the other hand, an improperly low stiffness may lead to significant underestimation of the peak rotation of the deck. Therefore, when applying the compliance approach, one should carefully choose a stiff enough gap element, and take friction into account.

REFERENCES

[1] Saiidi M.S., Vosooghi A., Nelson R., Shake-table studies of a four-span reinforced concrete bridge. *Journal of Structural Engineering, ASCE*, **139(12)**, 1352-1361, 2013.

[2] Buckle I., Hube M., Chen G., Yen W., Arias J., Structural performance of bridges in the Offshore Maule earthquake of 27 February 2010, *Earthquake Spectra*, **28(S1)**, S533-S552, 2012.

[3] Priestley, M. N., Seible, F., Calvi, G. M, *Seismic design and retrofit of bridges*, John Wiley & Sons, 1996.

[4] Maragakis E. A., Jennings P. C., Analytical models for the rigid body motions of skew bridges. *Earthquake Engineering & Structural Dynamics*, **15**, 923-944, 1987.

[5] Kaviani P., Zareian F., Taciroglu E., Seismic behavior of reinforced concrete bridges with skew-angled seat-type abutments. *Engineering Structures*, **45**, 137-150, 2012.

[6] Jankowski F., Wilde K., Fujino Y., Pounding of superstructure segments in isolated elevated bridge during earthquakes, *Earthquake Engineering & Structural Dynamics*, **27**, 487-502, 1998.

[7] Amjadian M., Agrawal A., Rigid-body motion of horizontally curved bridges subjected to earthquake-induced pounding, *Journal of Bridge Engineering, ASCE*, **21(12)**, 2016.

[8] Dimitrakopoulos E. G., Analysis of a frictional oblique impact observed in skew bridges, *Nonlinear Dynamics*, **60**, 575-595, 2010

[9] Dimitrakopoulos E. G., Seismic response analysis of skew bridges with pounding deck-abutment joints, *Engineering Structures,* **33(3)**, 813–826, 2011

[10] Dimitrakopoulos E. G., Nonsmooth analysis of the impact between successive skew bridge-segments, *Nonlinear Dynamics*, **74**, 911-928, 2013

[11] Shi Z., Dimitrakopoulos E. G., Nonsmooth dynamics prediction of measured bridge response involving deck-abutment pounding, *Earthquake Engineering & Structural Dynamics*, DOI: 10.1002/eqe.2863, 2017

[12] Leine R. I., Van Campen D. H., Glocker C. H., Nonlinear dynamics and modeling of various wooden toys with impact and friction. *Journal of Vibration Control*, **9(1–2)**, 25–78, 2003.

[13] Glocker C., *Set-Valued Force Laws*, Springer, 2001.

[14] Brogliato B., *Nonsmooth mechanics: models, dynamics and control*, Springer, 2016.

[15] Cottle R., Pang J., Stone R. E., *The linear complementarity problem*, Academic Press, 1992.

[16] Takeda T., Sozen M. A., Nielsen N. N., Reinforced concrete response to simulated earthquakes. *Journal of Structural Division, ASCE*, **96(12)**, 2557-2573, 1970.

[17] Goldsmith W., *Impact: The Theory and Physical Behaviour of Colliding Solids*, Edward Arnold, London, 1960.

[18] Muthukumar S., DesRoches R., A hertz contact model with non-linear damping for pounding, *Earthquake Engineering & Structural Dynamics*, **35**, 811-828, 2006.

[19] Lankarani H. M., Nikravesh P. E., A contact force model with hysteresis damping for impact analysis of multibody systems, *Journal of Mechanical Design (ASME)*, **112**, 354-374, 1990.